ISSN 0031-918X, Physics of Metals and Metallography, 2020, Vol. 121, No. 13, pp. 1339–1346. © Pleiades Publishing, Ltd., 2020.

STRENGTH AND PLASTICITY

Residual Stresses and Microstructural Features of Rotary-Friction-Welded from Dissimilar Medium Carbon Steels

Elena Priymak[a, b, *], Zakaria Boumerzoug[c], Anna Stepanchukova[a], and Vincent Ji[d]

[a] *ZBO Drill Industries, Prospect Pobedi 118, Orenburg, 460026 Russia*

[b] *Orenburg State University, Prospect Pobedi 13, Orenburg, 460018 Russia*

[c] *Department of Mechanical Engineering, LMSM, University of Biskra, B.P. 145, Biskra-07000 Algeria*

[d] *University Paris-Sud 11, ICMMO/SP2M UMR CNRS 8182, Orsay, F-91405 France*

**e-mail: elena-pijjmak@yandex.ru*

Received September 19, 2019; revised February 4, 2020; accepted February 27, 2020

Abstract—The purpose of the present study was to fulfill the knowledge gap concerning the residual stress distribution in dissimilar medium carbon steels welded by a rotary friction technique. For this purpose, residual stresses were evaluated by X-ray diffraction. Microstructure observations, microhardness measurements and tensile tests were performed to couple all information. In addition, the distribution of residual stresses was evaluated in welded samples heat treated at 300 and 600°C. We have found that the residual stress distribution is in the high compression in thermomechanical affected zones, due to the microstructural changes during the welding process. Two subzones form the thermomechanical affected zone. However, the heat treatments caused a relaxation phenomenon in the weld region which is due to the recrystallisation during the heat treatments.

Keywords: rotary friction welding, medium carbon steels, post-weld heat treatment, thermomechanical affected zone, residual stresses, microstructure, mechanical properties

DOI: 10.1134/S0031918X20130165

INTRODUCTION

Rotary friction welding (RFW) is one of the solid state joining techniques which is applied to assemble similar and/or dissimilar materials. This technology has a lot of advantages over other welding processes. These advantages are no melting, high reproducibility, short production time, low energy input, limited heat affected zone, avoidance of porosity formation, no grain growth and the use of non-shielding gasses during the welding process [1–3]. In the process of RFW, two components with circular cross section are welded together. One part is held stationary and forced to come into contact with the other, which is rotating under normal pressure. The parts which are to be assembled are brought together for some time with a specified pressure, causing friction to be produced between the parts, and they undergo plastic deformation. Then the rotated part is suddenly stopped and pressure is applied until they produce a weld or joint.

During welding by RFW, rapid heating and cooling takes place which produces a severe thermal cycle near the weld line. This affected zone of the base metal is called the Thermomechanical Affected Zone (TMAZ). The TMAZ is the zone where heat transfers from the weld metal to the base metal. As a result, the welded joint obtained by RFW is a structurally inhomogeneous zone, characterised by a wide spectrum of formed structures and stresses. The phenomenon of residual stress can occur due to two factors: the mechanical deformation factor and the temperature gradient factor [4]. Although a large amount of previous studies [5–11] on the friction welding of similar and dissimilar materials has been conducted, limited studies have investigated the impact of friction welding on the residual stress distribution in the welded joint [12–25]. Similar studies can be found for friction stir welding [4, 14–19] and linear friction welding [20–24], which is the most similar to the formation mechanism of rotary friction welding, and RFW [25].

For example, Gan et al. [25] found that relatively high tensile residual stresses were observed near the bond line on the AA7020-T6 side, welded to 316L steel by RFW. They found a heterogeneous distribution of residual stresses from the perimeter to the rod centre, while high compressive residual stresses were found in the sample centre at the bond line in the 316L steel. Delijaicov et al. [4] studied the effect of the welding parameter variations on residual stresses of dissimilar butt joints of AA2024-T3 and AA7475-T761 joined by friction stir welding. They found that the increase of longitudinal and transverse residual stresses starts at the TMAZ due to shoulder pressure at the joint.

Investigation of RFW of two dissimilar steels, 32-2Mn and 40-Cr–Ni, is important, because these

Table 1. The chemical composition of the welded materials

Material	C	Mn	Si	S	P	Cr	Ni	Cu	Mo
32-2Mn	0.32	1.07	0.18	0.002	0.006	0.09	0.10	0.17	0.02
40-Cr–Ni	0.31	0.53	0.32	0.006	0.004	0.51	1.06	–	0.09

two steels are used for the production of geological exploration drill pipes [26]. A previous investigation [26] focussed on the post-weld tempering effect on the mechanism of fracture of welded joints of these medium alloy steels. However, an investigation of the residual stresses in rotary friction welded joints from these dissimilar materials has not been reported up-to-date. Thus, the main objective of this research is directed to the establishment of the residual stress distribution in medium carbon steel welded joints made by rotary friction welding, and also after the application of post-weld heat treatment.

MATERIALS AND METHODS

Medium carbon steels 32-2Mn and 40-Cr–Ni, were chosen to be welded by a friction rotary technique. The chemical composition of the welded materials is shown in Table 1.

The friction welding of pipe billets with a diameter of 63.5 mm and a wall thickness of 4.5 mm is shown in Fig. 1. The experimental samples were produced on a Thompson-60 friction welding machine. The welding process is carried out in several stages. The welded blanks are installed in stationary clamps and one of them is rotated. The blanks are held together and heated up to a temperature necessary for the formation of a welded joint (1000–1300°C). Then the rotation is quickly stopped, and an axial forging force is applied to the blanks. In this investigation, the welding parameters were as follows: friction force 50 kN, forging force 130 kN, friction time 5.86 s, burn-off length 8 mm, and rotation speed 800 rpm. Figure 1 shows the welding of 32-2Mn steel to 40-Cr–Ni steel.

Tensile tests were performed using a tensile testing machine R-50 with a constant strain rate of 0.021 m s^{-1}. Tensile test specimens were prepared according to ASTM E8. Tensile strength, yield strength and elongation of the welded specimens were determined. Hardness values (HV) were measured by using an HVS-1000 device with a load of 2 N for 10 s. The precision of measuring the diagonal of the print was ± 0.2 μm. For the tensile strength, three specimens were used. The microstructure was investigated using a Nikon ECLIPSE 10 optical microscope. The Microstructure of the different zones of the weld material, i.e. the weld seam, thermomechanical affected zone (TMAZ), and the base metal were revealed after etching by Nital.

X-ray stress measurements were carried out using SET-X equipment. Cr$K\alpha$ radiation (wavelength = 0.229 nm) and {211} reflections (Bragg angle = 156.3°) were used to study the residual stress distribution in the weld region of the welded samples. Stress measurements were made in the longitudinal and transverse directions (parallel and perpendicular to the weld joint, respectively). The X-ray diffraction depth is about 6 microns from sample surface. The stress analysis was carried out according to European standard EN 15305 (Test Method for Residual Stress analysis by X-ray Diffraction, April 2009). The $\sin^2\psi$ method was used for stress evaluation. For each stress determination, 13 different Psi angles (variant from −37° to +37°) were used.

The radiocrystallographic constants used $1/2\ S_{2\{211\}}$ and $S_{1\{211\}}$, are 5.83×10^{-6} and -1.28×10^{-6} MPa^{-1}, respectively. To study the effect of post-weld heat treatment on the distribution of residual stresses in the friction welded joints, heat treatment of the welds was carried out in an induction heating unit. The heating temperatures were 300 and 600°C for a duration of 60 s.

RESULTS AND DISCUSSION

Microstructural Observations

Base metals. The microstructure of the two dissimilar base metals is shown in Fig. 2. In the 32-2Mn steel

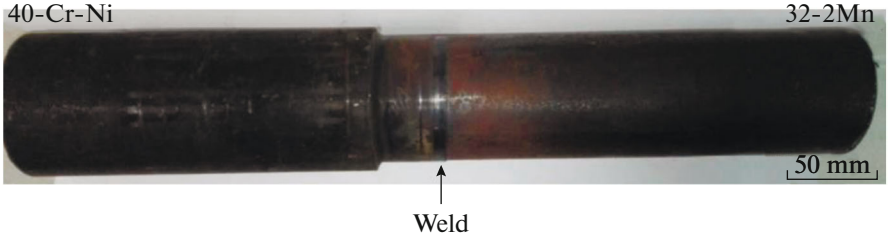

Fig. 1. The welding of 32-2Mn steel to 40-Cr–Ni steel by RFW process.

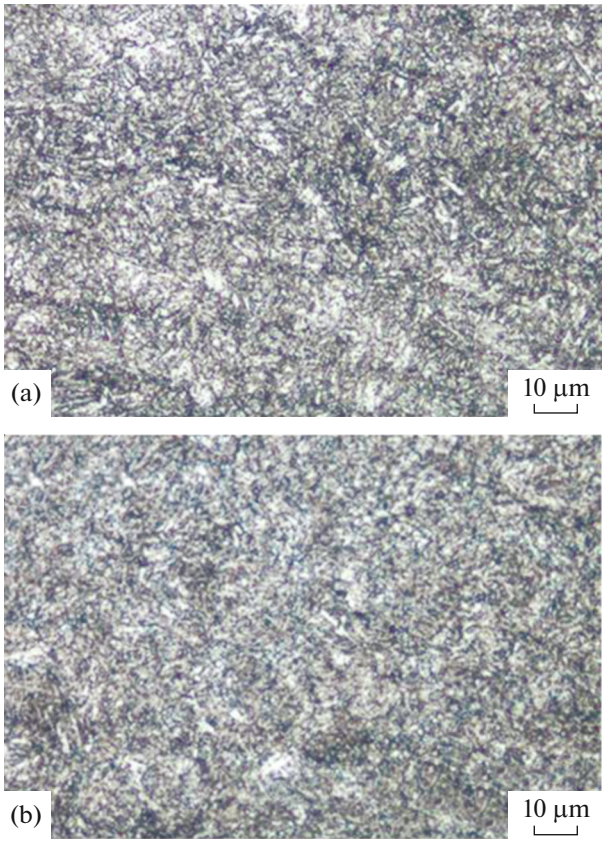

Fig. 2. Microstructure of the base metals: (a) 32-2Mn, and (b) 40-Cr–Ni.

the main phases are fine bainite with a mixture of ferrite and cementite. In the 40-Cr–Ni steel the main phases are a fine martensite structure.

Welded dissimilar steels. The macrostructure for the cross-section of the rotary friction welded joint is presented in Fig. 3. First of all, the weld interface clearly shows the line of the joint. In both sides, the main observed zones of the welded joint are the base metal and the thermomechanical affected zone (zone I + II), separated by the contact line. In the TMAZ, two main sub-zones can be distinguished in the two sides of the welded joint:

—sub-zone (I) is due to deformations and temperatures exceeding the critical point of A_{c3}.

—sub-zone (II) is due to local deformations.

The macrostructure of sub-zone I in the 32-2-Mn side is different to the 40-Cr–Ni side. This subzone I is the area of the dynamic recrystallisation reaction. However, the macrostructure of the subzone II in both sides of the welded joint seems similar. This subzone II reflects the high plastic deformation effect on both base metals.

Figure 4 presents the microstructure of the welded joint at the contact line which shows more details. The contact line is a boundary oriented in the contact plane. In some parts of the contact line, the formation of common grains is visible. This suggests that during rotational welding the interaction in the junction zone at some sites is not limited to the formation of interatomic bonds, but also to the mutual bulk recrystallisation.

Near the contact line in both steels the microstructure is complex, consisting mainly of ferrite (F), martensite (M) and bainite (B). The main observed ferrites are intergranular polygonal ferrite (PF), grain boundary ferrite (GF) and acicular ferrite (AF). There is a difference of the grain size due to the abnormal growth of some grains, which implies a consistent development of dynamic recrystallisation during the welding process.

The observed complex microstructure found in both steels was according to the nomenclature from the "Compendium of weld metal microstructures and properties" work from TWI [27]. Cheng et al. [28] indicated that when the peak temperature was higher

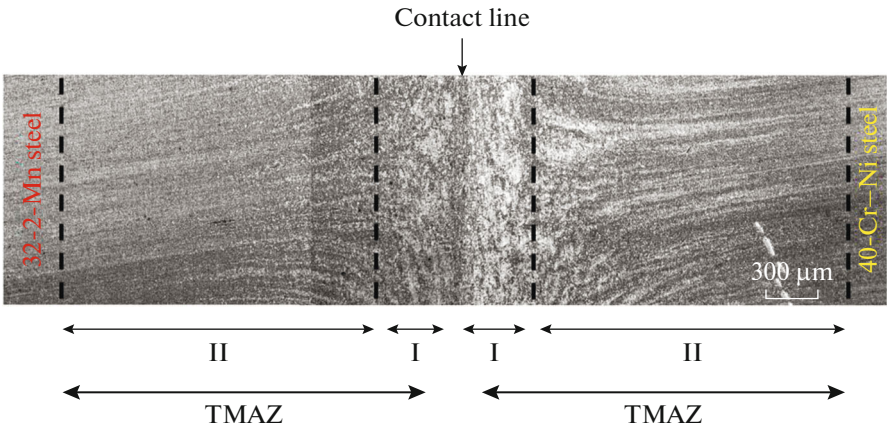

Fig. 3. Macrostructure of the rotary friction welded joint and the distinct sub-zones I, II, on both sides of the contact line: 32-2-Mn/40-Cr–Ni.

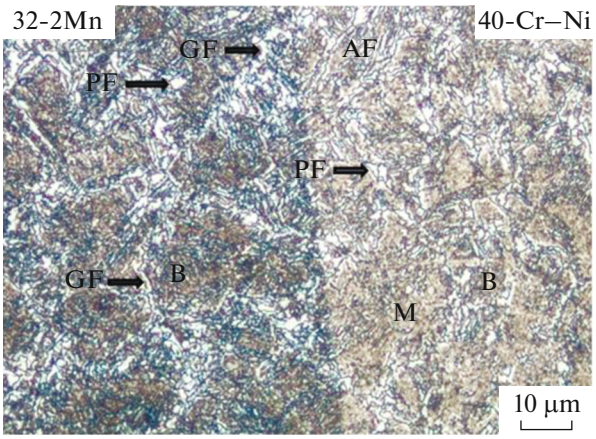

Fig. 4. Microstructure of the welded joint at the contact line. (GF: grain boundary ferrite, PF: polygonal ferrite, AF: acicular ferrite, M: martensite, B: bainite.)

than the eutectoid temperature (A_1), the microstructure of high carbon steel due to the friction welding process consisted mainly of martensite. However, when the welding was performed below A_1, no transformation occurred and no martensite was formed [29].

Figure 5 shows the microstructure of each sub-zone I and II in both sides of the welded joint. Concerning the TMAZ in 40-Cr–Ni steel, in the sub-zone I, which is the area adjacent to the welded joint, coarse grains were formed with a complex mixed microstructure consisting mainly of ferrite, martensite and bainite. The sub-zone II is formed with finer grains which indicates the intensive development of the recrystallisation processes in this zone. This recrystallisation reaction was due to heating and deformation during the friction process. The microstructure of the two sub-zones in TMAZ of 32-2-Mn steel are similar to those observed previously in TMAZ of 40-Cr–Ni steel, i.e., the subzone I formed with coarse grains and sub-zone II contains finer grains.

Heat treatment of the welded steels. By increasing the heating temperature from 300 to 600°C, the macrostructure of the TMAZ in both sides of the welded joint becomes more homogeneous, and the two distinct sub-zones disappear in the dissimilar steels. In addition, the welded joint becomes homogeneous with the base metal.

Microstructural observations of the different sub-zones in the welded joints of dissimilar steels after heat

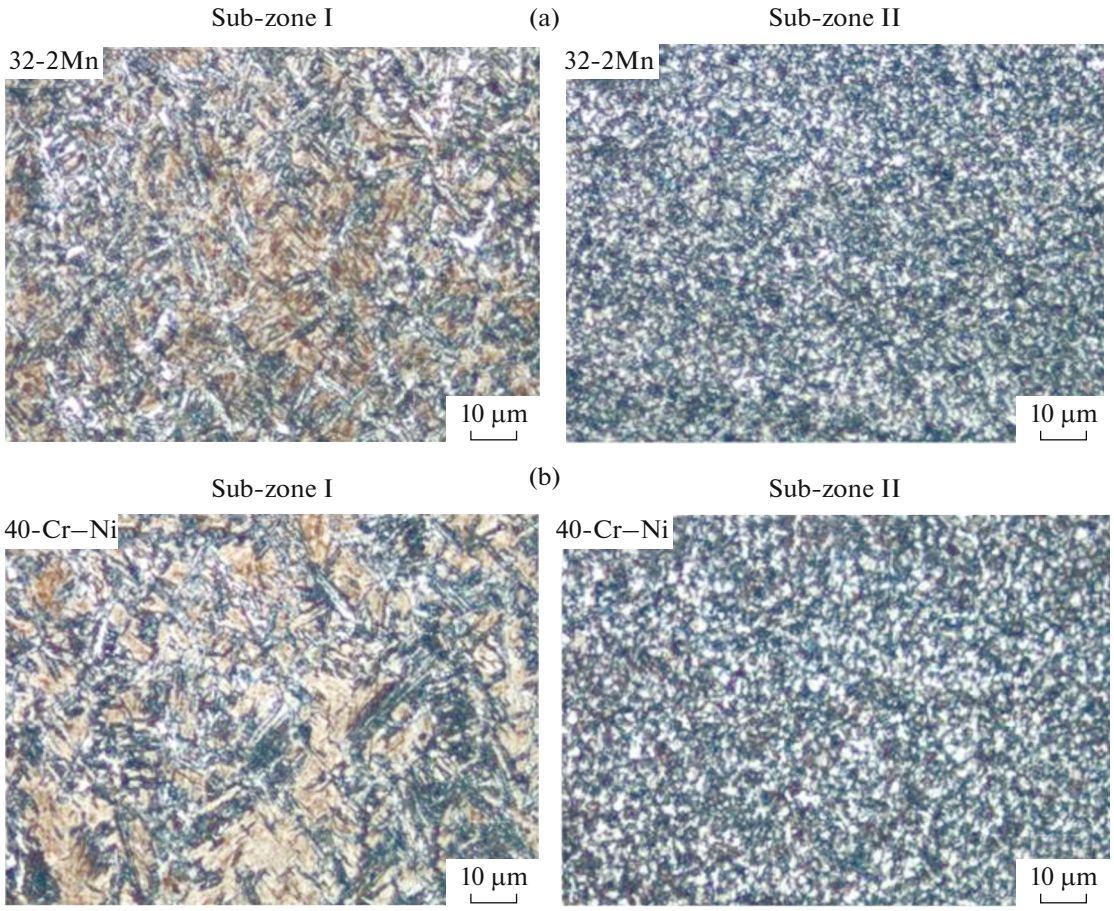

Fig. 5. Microstructures of the two sub-zones I and II of the TMAZ in (a) 32-2-Mn steel and (b) 40-Cr–Ni steel.

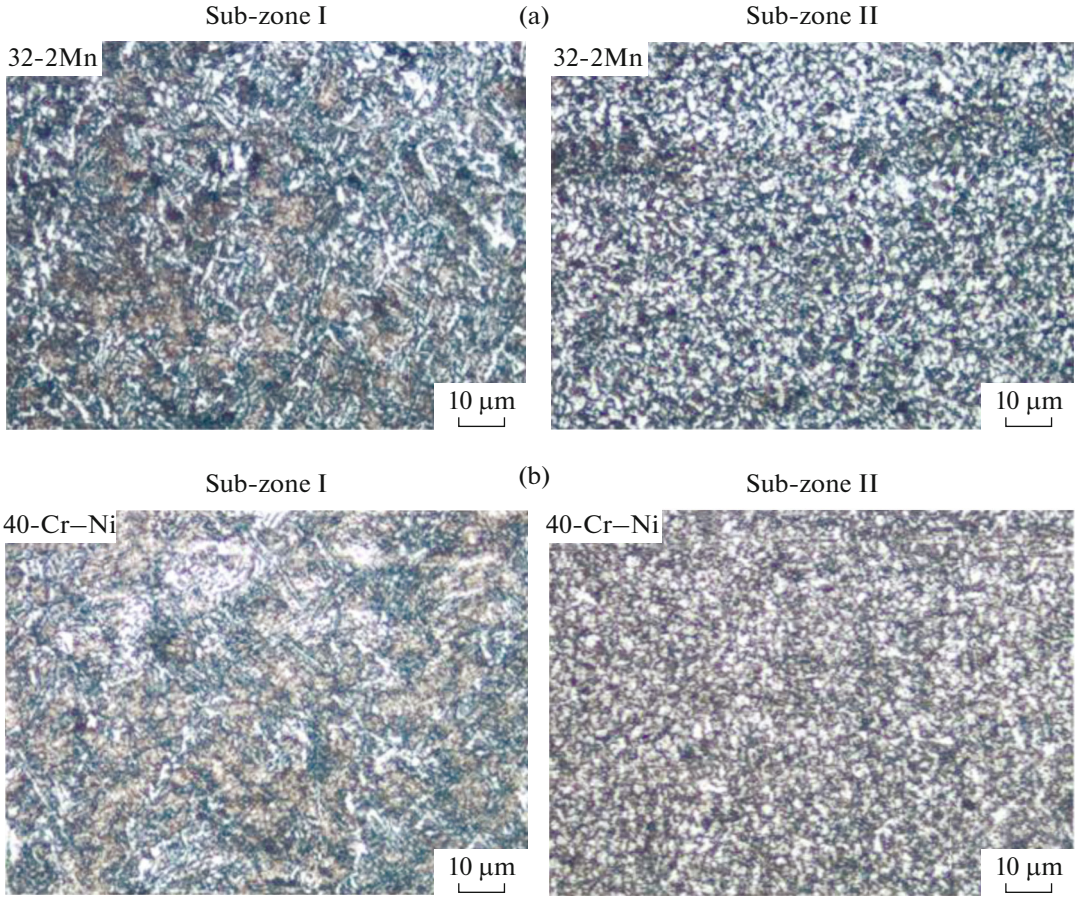

Fig. 6. Microstructure of the rotary friction welded joint after post-heat treatment 600°C during 60 s in (a) 32-2-Mn and (b) 40-Cr–Ni.

treatment at 600°C (Fig. 6) reveal that the post-welding heat treatment leads to a homogenisation of the microstructure in TMAZ, and there is only a slight difference between the two sub-zones in both sides of the welded joint. This transformation is mainly due to the recrystallisation reaction.

Microhardness Measurements

Hardness measurements were performed on the welded joint before and after isothermal heat treatment at 300 and 600°C. Concerning the weld joint before heat treatment, the microhardness results indicate that the nature of the change in microhardness over the length of the TMAZ corresponds to the structural changes caused by the thermal deformation effect of the welding process (Fig. 7).

However, hardness values of the two base metals were unchanged because they are not affected by the heat generated while welding. The formation of both hardened and weakened areas can be seen in TMAZ, which is probably due to the existence of two distinct sub-zones in TMAZ. In addition to these sub-zones, the different phases formed in TMAZ, such as the presence of the martensitic and bainite phases, explains the high hardness in sub-zone I adjacent to the contact line. Values measured in this area ranged from 267 to 323 HV. However, with increasing distance from the contact line, the microhardness values decreased smoothly, reaching a minimum in the recrystallisation development zone.

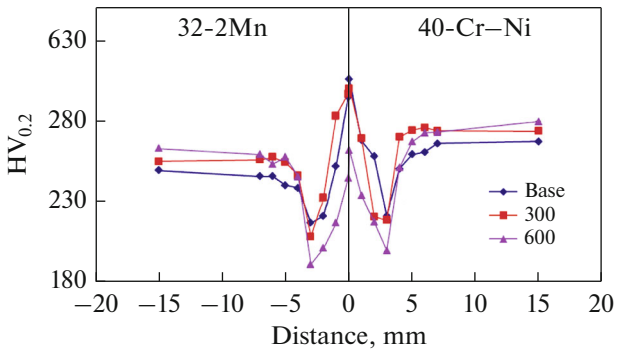

Fig. 7. Hardness measurement profiles of weld joint 32-2Mn/ 40-Cr-Ni, before and after post-weld heat treatment at 300 and 600°C.

Table 2. Tensile tests properties of the joint weld 32-2Mn and 40-Cr–Ni before and after heat treatment at 300 and 600°C

Type of joint weld	Yield strength $\sigma_{0.2}$, MPa	Tensile strength σ_u, MPa
After welding	843+/–8.4	892+/–8.9
300°C	834+/–8.3	887+/–8.9
600°C	734+/–7.3	808+/–8.1

The post-weld heat treatment at 300°C had practically no effect on the level of microhardness values. With an increase in the heating temperature up to 600°C, the microhardness profile remained the same, but there was a decrease in the microhardness values in all TMAZ zones, and in the centre of the welded joint, which corresponds to the zones adjacent to the contact line as mentioned in the microstructure observation. This decrease of hardness values in the welded joint corresponds to a softening phenomenon after heat treatment at 600°C which can be attributed to the martensite transformation to a softer phase, and also to the recrystallisation reaction.

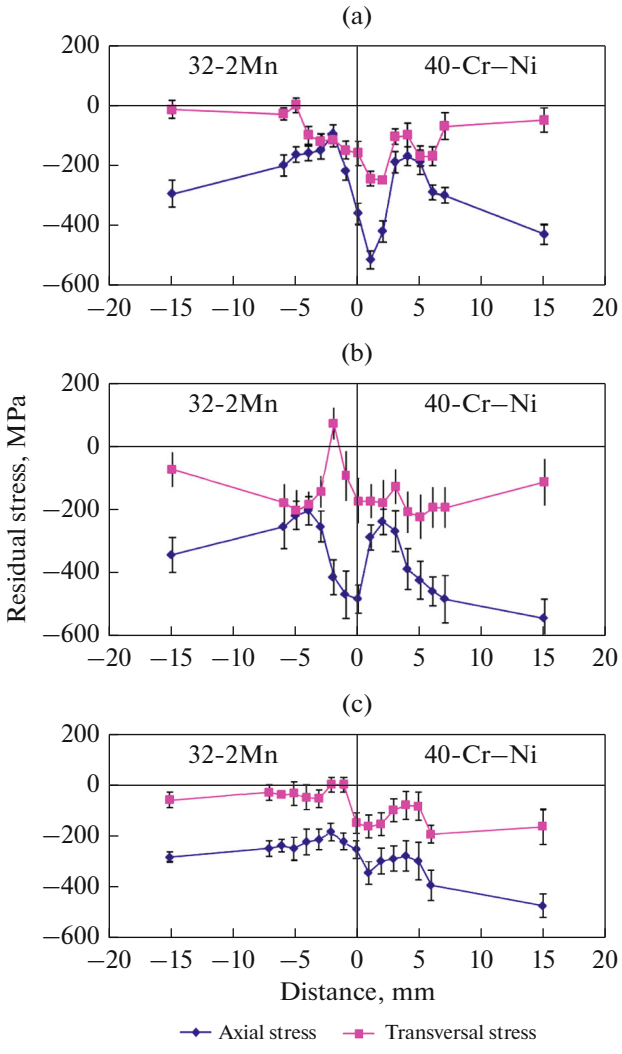

Fig. 8. Residual stress in the rotary friction weld from medium carbon steels: (a) after welding; (b) after post-weld heat treatment at 300°C; (c) after post-weld heat treatment at 600°C.

Tensile Tests

Friction welding enables the joining of materials giving a weld of high strength with many advantages over the other welding processes. Table 2 presents the results of tensile tests performed on welded samples before and after heat treatment at 300 and 600°C.

Based on these results, the welded sample has the highest tensile strength (892 MPa) and highest yield strength (892 MPa) with a slight decrease of these values after heat treatment at 300°C. However, the heat treatment at 600°C decreases the tensile strength to 808 MPa and also the yield strength to 734 MPa. This decrease of the mechanical properties after heat treatment at 600°C confirms the softening phenomenon. As mentioned above, this softening phenomenon is due to the recrystallisation reaction developed in the welded joint at this high temperature and also to the occurrence of new soft phases.

Residual Stress Distribution

Longitudinal and transverse residual stress distributions in the rotary friction welded joint, before and after heat treatment at 300 and 600°C, are shown in Fig. 8. Concerning the weld joint before heat treatment, we can deduce from Fig. 8a that the residual stress distribution in the welded joint is opposed to the hardness profile.

As presented in Fig. 8a, the lowest values of residual stresses are measured in the contact line. These hard zones are subjected to a temperature gradient imposed by the welding thermal cycle.

Compressive residual stresses in two directions were observed in TMAZ and the base metal. The results indicate that in the contact line the value of stress is –360 MPa in the longitudinal direction, and –160 MPa in the transverse direction. The maximum compressive residual stresses are at 1 mm from the contact line in 40-Cr–Ni (–515 MPa) in the longitudinal direction (Fig. 8a). Moreover, the residual stress profile across the welded joint displays an ‘M’ trend with varied degrees of intensity, which is characteristic of friction stir joints [13–16].

After tempering at 300°C, the axial stresses are little changed. On the other hand, in the transverse direction, the residual stresses in the TMAZ have been relaxed and are close to zero (Fig. 8b). After tempering at 600°C, the stresses are more or less relaxed in both directions and in the different zones (in the centre of

the welded and the TMAZ) (Fig. 8c). Iqbal et al. [30] found that the residual stresses in post-weld heat treated friction welded nickel-based superalloys were about 35% less than for the as-welded condition. This result confirms the softening phenomenon in the welded joint after heat treatment at 600°C.

CONCLUSIONS

Our investigation represents a contribution to the study of the distribution of residual stresses in the rotary friction welding of dissimilar metallic materials. Two different medium carbon steels were welded by the rotary friction welding process and submitted to post-welding heat treatment at 300 and 600°C. The characterisation of the welded joint before and after heat treatment has revealed the following conclusions:

—The thermomechanical affected zone is divided into two sub-zones in both sides of the welded joint.

—These two subzones have an effect on the hardness profile across the welded joint.

—A softening phenomenon was developed in the welded joint after heat treatment at high temperature (600°C).

—The macrostructural and microstructural observations revealed that the heat treatment at 600°C for 60 seconds was sufficient to obtain a homogeneous welded joint with the base metal.

—Stress distribution in the welded joint is characterised by high compressive stresses in the thermomechanical affected zone due to the microstructural changes present in the cross-section of the welds. However, the heat treatments caused a relaxation phenomenon in the weld region which is due to the recrystallisation reaction caused by the heat treatment.

REFERENCES

1. N. Shete and S.U. Deokar "A review, paper on rotary friction welding," *Int. Conf. on Ideas, Impact and Innovation in Mechanical Engineering. (ICIIIME)*. **5**, 1557–1560 (2017).
2. W. Y. Li, A. Vairis, M. Preuss, and T. J. Ma, "Linear and rotary friction welding review," Int. Mater. Rev. **61**, 71–100 (2016).
3. M. Maalekian, "Friction welding–critical assessment of literature," Sci. Technol. Weld Joining **12**, 738–759 (2007).
4. S. Delijaicova, P. A. de O. Silvaa, H. B. Resendeb, and M. H. F. Batalhab, "Effect of weld parameters on residual stress, hardness and microstructure of dissimilar AA2024-T3 and 3AA7475-T761 friction stir welded joints," Mater. Res. **21**, (2018).
5. M. Sahin, "Joining with friction welding of high- speed steel and medium-carbon steel," J. Mater. Process. Technol. **168**, 202–210 (2005).
6. M. Sahin, "Characterisation of properties in plastically deformed austenitic-stainless steels joined by friction welding," Mater. Des. **30**, 135–144 (2009).
7. M. Sahin, "Evaluation of the joint-interface properties of austenitic-stainless steels (AISI 304) joined by friction welding," Mater. Des. **28**, 2244–2250 (2007).
8. N. O. Zdemira, F. Sarsılmaz, and A. Hascalık, "Effect of rotational speed on the interface properties of friction welded AISI 304L to 4340 steel," Mater. Des. **28,** 301–307 (2007) .
9. S. T. Selvamani1, K. Umanath, K. Palanikumar, et al., "The microhardness analysis of friction welded AISI 52100 grade carbon steel joints," Adv. Mater. Res. **984–985**, 613–617 (2014).
10. V. V. Satyanarayana, R. G. Madhusudhan, and T. Mohandas, "Dissimilar metal friction welding of austenitic–ferritic stainless steels," J. Mater. Process. Technol. **160**, 128–137 (2005).
11. N. S. Kalsi, and V. S. Sharma, "A statistical analysis of rotary friction welding of steel with varying carbon in workpieces," Int. J. Adv. Manuf. Technol. **57,** 957–967 (2011).
12. G. V. B. Lemos, P. H. C. P. Cunha, R. M. Nunes, et al., "Residual stress and microstructural features of friction-stir-welded GL E36 shipbuilding steel," Mater. Sci. Technol. **34**, 95–103 (2018). https://doi.org/10.1080/02670836.2017.1361148
13. A. Steuwer, S. J. Barnes, J. Altenkirch, et al., "Friction stir welding of HSLA-65 steel: part II. The influence of weld speed and tool material on the residual stress distribution and tool wear," Metall. Mater. Trans. A **43**, 2356–2365 (2012).
14. M. Peel, A. Steuwer, M. Preuss, et al., "Microstructure, mechanical properties and residual stresses as a function of welding speed in aluminium AA5083 friction stir welds," Acta Mater. **51**, 4791–4801 (2003).
15. L. N. Brewer, M. S. Bennett, B. W. Baker, et al., "Characterisation of residual stress as a function of friction stir welding parameters in oxide dispersion strengthened (ODS) steel MA956," Mater. Sci. Eng., A **647**, 313–321 (2015).
16. M. Z. Khandkar, J. A. Khan, A. P. Reynolds, et al., "Predicting residual thermal stresses in friction stir welded metals," J. Mater. Process. Technol. **174**, 195–203 (2006).
17. G. Bufa, L. Frantini, and S. Pasta, "Residual stresses in friction stir welding: numerical simulation and experimental verification," *Invited paper at ICRS-8 8th International Conference on Residual Stresses* (Colorado, 2008).
18. N. Kumar, R. S. Mishra, and J.A. Baumann, Residual Stresses in Friction Stir Welding (Oxford, 2014), p. 50.
19. A. P. Reynold, W. Tang, T. Gnaupel-Herold, et al., "Structure, properties, and residual stress of 304L stainless steel friction stir welds," Scr. Mater. **48**, 1289–1294 (2003).
20. R. Nikiforov, A. Medvedev, E. Tarasenko, et al., "Numerical simulation of residual stresses in linear friction

welded joints," J. Eng. Sci. Technol. Rev. **8**, 49–53 (2015).

21. C. Bühr, B. Ahmad, P. A. Colegrove, et al., "Prediction of residual stress within linear friction welds using a computationally efficient modelling approach," Mater. Des. **139**, 222–233 (2018).
22. J. Romero, M. Attallah Moataz, M. Preuss, et al., "Effect of the forging pressure on the microstructure and residual stress development in Ti–6Al–4V linear friction welds," Acta Mater. **57**, 5582–5592 (2009).
23. P. Xie, H. Zhao, and Y. Liu, "Measuring residual stresses in linear friction welded joints composed by dissimilar titanium," Sci. Technol. Weld. Joining **21** (5), 351–357 (2016).
24. Y. Fu, W. Y. Li, X. W. Yang, et al., "The effects of forging pressure and temperature field on residual stresses in linear friction welded Ti6Al4V joints," Adv. Manuf. **4**, 314–321 (2016).
25. W. M. Gan et al. "Microstructure and residual stress in rotary friction welded dissimilar metals of AA7020 aluminium alloy with 316L steel," Mater. Sci. Forum **879**, 572–577 (2017).
26. E. Priymak, A. Atamashkin, and A. Stepanchukova, "Effect of post-weld heat treatment on the mechanical properties and mechanism of fracture of joint welds made by Thompson friction welding," Mater. Today: Proc. **11**, 295–299 (2019).
27. "Compendium of weld metal microstructures and properties: submerged-arc welds in ferritic steel: prepared for Commission IX of the International Institute of Welding by sub-commission IXJ". (Abington, The Welding Institute, 1985).
28. C. P. Cheng, H. M. Lin, and J. C. Lin, "Friction welding of ductile iron and low carbon steel," Sci Technol. Weld. Joining **15**, 706–711 (2010).
29. H. Fujii, L. Cuia, N. Tsuji, et al., "Friction stir welding of carbon steels," Mater. Sci. Eng., A **429**, 50–57 (2006).
30. N. Iqbal, J. Rolph, R. Moat, et al., "A comparison of residual stress development in inertia friction welded fine grain and coarse grain nickel-base superalloy," Metall. Mater. Trans. A **42**, 4056–4063 (2011).